Electron-Induced Oxygen Desorption from the TiO2 (011)-2x1 Surface Leads to Self-Organized Vacancies

Olga Dulub, *et al.*

Science **317**, 1052 (2007);
DOI: 10.1126/science.1144787

Science (print ISSN 0036-8075; online ISSN 1095-9203) is published weekly, except the last week in December, by the American Association for the Advancement of Science, 1200 New York Avenue NW, Washington, DC 20005.

18. L. P. Regnault, I. A. Zaliznyak, J. P. Renard, C. Vettier, *Phys. Rev. B* **50**, 9174 (1994).
19. Th. Jolicur, O. Golinelli, *Phys. Rev. B* **50**, 9265 (1994).
20. M. T. Hutchings, G. Shirane, R. J. Birgeneau, S. L. Holt, *Phys. Rev. B* **5**, 1999 (1972).
21. J. Skalyo Jr., G. Shirane, R. J. Birgeneau, H. J. Guggenheim, *Phys. Rev. B* **2**, 4632 (1970).
22. S. Itoh, Y. Endo, K. Kakurai, H. Tanaka, *Phys. Rev. Lett.* **74**, 2375 (1995).
23. A. V. Sologubenko, T. Lorenz, H. R. Ott, A. Freimuth, *J. Low Temp. Phys.* **147**, 387 (2007).
24. K. Kordonis, A. V. Sologubenko, T. Lorenz, S.-W. Cheong, A. Freimuth, *Phys. Rev. Lett.* **97**, 115901 (2006).
25. A. P. Ramirez, S.-W. Cheong, K. L. Kaplan, *Phys. Rev. Lett.* **72**, 3108 (1994).
26. M. Yoshida *et al.*, *Phys. Rev. Lett.* **95**, 117202 (2005).
27. K. Damle, S. Sachdev, *Phys. Rev. B* **57**, 8307 (1998).
28. T. Sakaguchi, K. Kakurai, T. Yokoo, J. Akimitsu, *J. Phys. Soc. Jpn.* **65**, 3025 (1996).
29. A. Zheludev *et al.*, *Phys. Rev. B* **53**, 15004 (1996).
30. M. Kenzelmann, R. A. Cowley, W. J. L. Buyers, D. F. McMorrow, *Phys. Rev. B* **63**, 134417 (2001).
31. M. P. Nightingale, H. W. J. Blöte, *Phys. Rev. B* **33**, 659 (1986).
32. We thank K. Damle, B. Keimer, S. Sachdev, S. Shapiro, and J. M. Tranquada for helpful discussions. Work in London was supported by a Wolfson–Royal Society Research Merit Award and the Basic Technologies program of Research Councils UK. Work at Johns Hopkins University, NIST, and Louisiana State University was supported by NSF and that at Brookhaven National Laboratory was supported by the Office of Science of the U.S. Department of Energy.

Supporting Online Material
www.sciencemag.org/cgi/content/full/1143831/DC1
Materials and Methods
Figs. S1 and S2
References

16 April 2007; accepted 12 July 2007
Published online 26 July 2007;
10.1126/science.1143831
Include this information when citing this paper.

Electron-Induced Oxygen Desorption from the TiO_2(011)-2×1 Surface Leads to Self-Organized Vacancies

Olga Dulub,[1] Matthias Batzill,[2] Sergey Solovev,[3] Elena Loginova,[3] Alim Alchagirov,[1] Theodore E. Madey,[3] Ulrike Diebold[1]*

When low-energy electrons strike a titanium dioxide surface, they may cause the desorption of surface oxygen. Oxygen vacancies that result from irradiating a TiO_2(011)-2×1 surface with electrons with an energy of 300 electron volts were analyzed by scanning tunneling microscopy. The cross section for desorbing oxygen from the pristine surface was found to be 9 (±6) × 10^{-17} square centimeters, which means that the initial electronic excitation was converted into atomic motion with a probability near unity. Once an O vacancy had formed, the desorption cross sections for its nearest and next-nearest oxygen neighbors were reduced by factors of 100 and 10, respectively. This site-specific desorption probability resulted in one-dimensional arrays of oxygen vacancies.

Desorption of atoms or molecules can occur when sufficient energy is available to overcome the potential barrier that forms the surface bond. Often this process occurs through thermal routes and the barrier is overcome through vibrational energy, but electronic transitions induced by photons or particles (typically electrons or ions) can lead to rapid desorption when the atom or molecule is excited to a higher-energy configuration that is repulsive in nature. This desorption induced by electronic transitions (DIET) has important fundamental and technological applications (*1*, *2*). DIET-related phenomena must be taken into account in areas as diverse as the modification of semiconductors (*3*), the radiation damage of optical materials (*4*, *5*), nuclear waste storage, and planetary science (*6*, *7*). By using the tip of a scanning tunneling microscope (STM) as an electron source, such processes can be used for the electronic control of single-molecule dynamics (*8*–*10*).

[1]Department of Physics, Tulane University, New Orleans, LA 70118, USA. [2]Department of Physics, University of South Florida, Tampa, FL 33620, USA. [3]Department of Physics and Astronomy and Laboratory for Surface Modification, Rutgers University, Piscataway, NJ 08855, USA.

*To whom correspondence should be addressed. E-mail: diebold@tulane.edu

Central to DIET phenomena is the efficient conversion of an initial electronic excitation into the motion of an atom. One of the earliest proposed mechanisms (*11*, *12*) invokes a Frank-Condon excitation of an adsorbate to a repulsive potential energy curve; under strong excitation conditions, such excitations can also be achieved by multiple electronic transitions (DIMET) (*13*). Desorption will occur only if the electronic excitation is long-lived and the nucleus starts to move before the excitation is quenched. Understanding the basic physics that quenches such excitations is important for technical applications, for example, in processes that convert solar energy into chemical reactions or electrical energy (*14*) or in contamination of optical elements in extreme ultraviolet lithography applications (*15*).

DIET processes differ from thermal desorption in several important ways. Surface species undergoing thermal desorption are close to equilibrium in that the vibrational energy can redistribute rapidly relative to the time scale of breaking surface bonds. Thermal desorption usually involves neutral species, but the much higher energies available in DIET processes allow charged species to leave the surface and overcome attractive forces, and cascading electron transfer processes can lead to desorption of anions, cations, metastables, and ground-state neutrals. Because thermal desorption processes are near to equilibrium, the effect of a desorption event on the remaining surface neighbors is a small perturbation; rapid diffusion will delocalize and randomize vacancies created by desorption. In DIET processes that occur far from equilibrium at low temperature, a vacancy created by desorption remains localized and cannot diffuse. One might expect that such immobile DIET-produced vacancies would be randomly arrayed on the surface.

We have investigated one of the canonical materials for studying DIET processes, TiO_2, and we find highly unusual and unexpected behavior for vacancy distributions on the (2×1) termination of TiO_2(011): Electron bombardment leads to formation of vacancy clusters, one-dimensional arrays of O vacancies. Why? Although the initial probability for O^+ desorption and the formation of an O vacancy is nearly unity, the creation of a vacancy markedly decreases the desorption probability of its nearest-neighbor and next-nearest-neighbor O atoms. The surface charge that accompanies defect formation must be the factor causing desorption probabilities to change so greatly.

Self-organization can be achieved where an initial process controls subsequent events. A string of such interrelated events can then lead to pattern formation. The unexpectedly high alteration of the desorption probability upon formation of an O vacancy is an example of this phenomenon; the initial desorption event is responsible for the self-organization of subsequent defects. This process should apply generally to DIET processes. Consequently, the formation of well-defined O-vacancy patterns must be taken into consideration in the radiation damage of insulating surfaces and can be used to enhance the chemical reactivity of DIET-modified surfaces.

We have investigated the effects of electron irradiation on TiO_2 not only because it has been a model system for DIET processes, but because it is a very promising material for solar energy conversion; it is also the prototypical material for fundamental studies of metal oxide surface reactivity (*16*, *17*). Its chemical, electronic, and optical properties depend strongly on the presence of steps, vacancies, and other surface defects

(*18*). It was recognized early on that electron-induced DIET processes remove oxygen from a TiO_2 surface (*19*). This allows control of the formation of O vacancies and modification of the surface reactivity on TiO_2 (*20*, *21*).

Knotek and Feibelman (K-F) proposed a mechanism for O^+ desorption from TiO_2 and other maximal-valence oxides (such as V_2O_5, WO_3, and NiO) (*19*). Their model is based on the interesting observation that the threshold energy for the electron-stimulated desorption (ESD) of O^+ from TiO_2 corresponds to the excitation energy of the Ti 3p core hole. To rationalize the formation of an O^+ ion from a (formally) O^{2-} species in the oxide lattice, it was proposed that the Ti core hole is filled with electrons from O 2p orbitals via an interatomic Auger process from a neighboring O atom. (It was argued that an intra-atomic Auger process, which is usually much faster, is not possible when the Ti 3d band is empty.) If three electrons escape from the oxygen, for example, in a double Auger decay, the O^{2-} ion becomes O^+. This O^+ ion can be ejected from the surface by Coulomb repulsion from the surrounding Ti^{4+} lattice ions.

The invoked double Auger decay is not a very likely process, however, and the K-F model ignores the high degree of covalency in TiO_2 (*22*) and many other transition metal oxides. Indeed, recent photo (Auger)–electron/ion coincidence spectroscopy measurements on TiO_2 (110) indicate that the K-F mechanism needs to be refined (*23*), because a Ti atom's initial and final states—before and after the core-hole excitation, respectively—contain mixtures of electron configurations that have one or more holes in a neighboring O atom. To date, there exists little information about the distribution of the O vacancies that result from electron irradiation (*20*), and no information that suggests self-organization.

We used STM to evaluate the effect of electron beam irradiation on a TiO_2(011)-2×1 surface. The (2×1) reconstruction of TiO_2(011) is produced by sputtering and thermal annealing to 1000 K. This surface is stable and stoichiometric, and its structure has been investigated extensively both experimentally and theoretically (*24*, *25*). The model of Fig. 1 is characterized by singly coordinated O atoms. Although details of bonding in the lowest-energy (2×1) structure are currently undergoing study (*26*), both STM (Fig. 2A) and all theoretical models to date confirm that O atoms are arranged in double rows with zigzag configuration. Whereas we display this structure in Fig. 1A because it appears to be consistent with experiment, other models with multiply coordinated O atoms are under evaluation (*26*). The desorbing species (O^+ and some H^+) have been monitored with a time-of-flight technique [electron-stimulated desorption ion angular distribution (ESDIAD) optics] and a quadrupole mass spectrometer. In the ESD process, ions are ejected at discrete angles determined by the orientation of the ruptured bonds (*2*). Figure 1B shows the angular distribution of O^+ ions desorbed from the surface. The ESDIAD pattern exhibits two off-normal emission lobes symmetric about the $[0\bar{1}1]$ direction.

Heating TiO_2 surfaces in vacuum produces O vacancies (*17*); the concentration of O vacancies typically amounts to 5 to 9% of surface O sites for the TiO_2(011) sample used. Such thermally induced defects appear as missing bright spots on TiO_2(011)-2×1 and do not show any apparent ordering (*25*). The TiO_2(011)-2×1 surface can sustain a large number of O vacancies without restructuring, which allows monitoring of O desorption over a large range of defect densities. This is different from the extensively investigated TiO_2(110) surface (*27*), which reconstructs after a maximum defect concentration of 10 to 12% is reached (*20*, *28*). Using the TiO_2(011)-2×1 surface instead of TiO_2(110) also has another practical advantage: Surface hydroxyl groups, which form readily when water dissociates at O vacancies, appear as brighter atoms in STM (*29*) and can be clearly distinguished from the black O vacancies on the TiO_2 (011)-2×1 surface. [The similarity of surface OH and O vacancies in STM images of TiO_2(110) can lead to ambiguities (*28*).]

After exposure to 300-eV electrons, ~55% of the surface O atoms had been desorbed (Fig. 2B). This desorption did not occur in a random fashion: Most of the remaining oxygen atoms were lined up along one side of the original zigzag row (yellow lines in Fig. 2B). These single-atom strands were up to 12 atoms long, whereas patches where the original zigzag configuration was preserved were much smaller. The defective surface was quite reactive; the very bright spots in Fig. 2B were caused by unknown impurities from the residual gas of the chamber that reacted with the defective surface.

The effect of electron irradiation is shown in more detail in Fig. 3, B to D. The vacancy concentration increased with increasing electron dose, up to a defect density of 70% of a monolayer (ML). (One monolayer of surface O

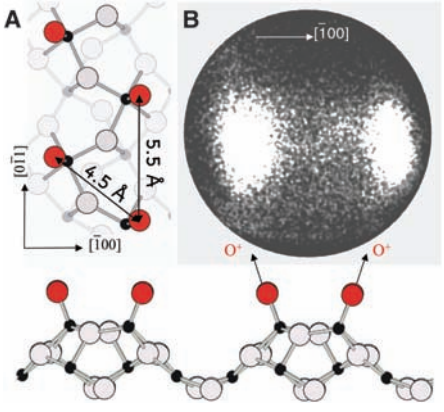

Fig. 1. (**A**) Model of the TiO_2(011)-2×1 surface. Titanium and oxygen atoms are represented as black and gray spheres, respectively; the red spheres represent one-fold coordinated surface oxygen atoms. The arrows in the side view illustrate the direction of O^+ ions when desorbed by an electron beam. (**B**) Experimental pattern of the angular O^+ ion distribution during electron-stimulated desorption from the TiO_2(011)-2×1 surface.

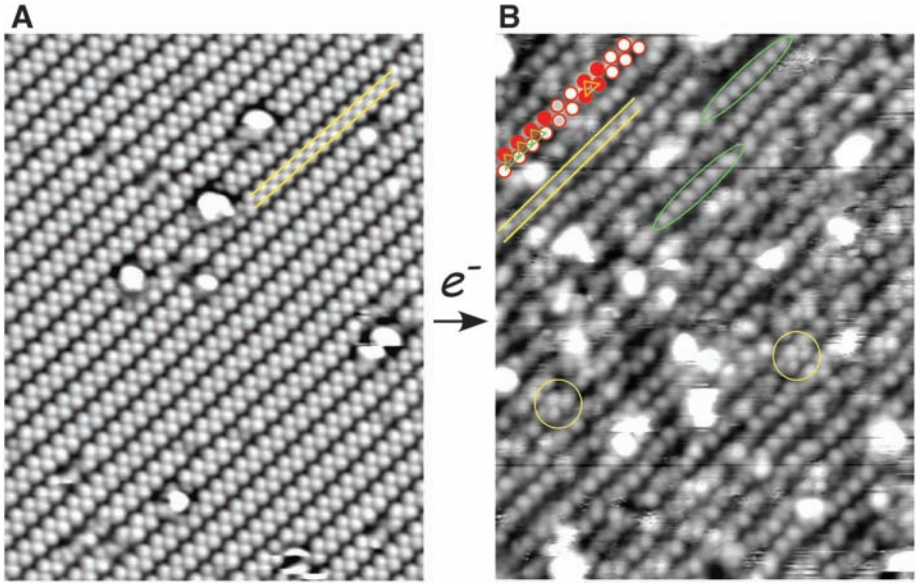

Fig. 2. (**A**) Scanning tunneling microscopy images (170 Å by 220 Å) of a clean TiO_2(011)-2×1 surface. Surface O atoms are arranged in double rows with a zigzag configuration; O vacancies appear as black spots. (**B**) The same surface after irradiation with 300-eV electrons, which causes the desorption of oxygen. Remaining O atoms are mainly arranged in one-dimensional strands along one side of the original double-row structure, as indicated by green ovals and yellow lines. Small areas that have maintained the original zigzag configuration are marked with yellow circles.

atoms corresponds to $N_0 = 4 \times 10^{14}$ atoms cm^{-2}.) Single-atom strands were observed for a wide range of doses (see Fig. 3 and the sketch of empty and filled O sites in Fig. 3G). Above a dose of 2.8×10^{17} electrons cm^{-2}, however, the surface became disordered in low-energy electron diffraction. Such surface vacancy arrays could not be created through thermal desorption; indeed, heating the electron-bombarded surface to 300°C in vacuo yielded the original, nearly stoichiometric surface.

In stimulated desorption a first-order process is often assumed, that is, a random removal of oxygen with a desorption cross section σ that does not change throughout the irradiation time. Figure 3F shows a Monte Carlo simulation of a typical distribution of 55% O vacancies that would result from a constant desorption cross section. (From the STM snapshot and the electron dose in Fig. 3C, a first-order desorption yield of one O per 420 incoming electrons was assumed.) The simulated arrangement of the remaining surface O atoms is very different from the one observed in the experiment (compare Fig. 3, C and G, with Fig. 3F). The characteristic, single-strand O rows that remain on one side of the original zigzags can only be attributed to a change in the desorption probability as vacancies are being formed. Moreover, for high densities of thermally induced point defects, such long single-atom strands were not observed, indicating that these do not represent a low-energy configuration. Hence, electron-stimulated diffusion (*30*) can be ruled out as a cause for the formation of the nonuniform distribution of O vacancies.

A site-dependent desorption process was modeled with a Monte Carlo simulation (Fig. 3H) with three adjustable parameters. The first parameter describes the probability for desorbing the first O atom from the pristine surface. Once a DIET-induced O vacancy has been produced, the probability for desorbing an O neighbor on the other side of the zigzag was reduced by a factor that was treated as the second parameter. One-dimensional strands could also be formed if the desorption probability for an oxygen neighbor on the same side of the zigzag row were increased; for some systems, an increased probability was indeed observed next to defects (*5*). Thus, the desorption probability for an O neighbor right next to a vacancy was treated as the third parameter in the simulations. As shown in Fig. 3G, a good qualitative agreement can be achieved with a desorption yield of 1:20 for the pristine surface, which is decreased by one and two orders of magnitude for oxygen neighbors adjacent to and opposite an existing O vacancy, respectively. In contrast, an increase in the desorption cross section for an O atom adjacent to an O vacancy does not result in the correct dose-dependent behavior.

To put these simulations on a more quantitative footing, we analyzed different vacancy configurations for a large number of images (total area 5×10^5 Å^2) obtained after various electron doses. Atoms in high-resolution STM images were binned in triangles, and three configurations were considered: (α) triangles with one atom filled and two sites empty (these are part of the single-atom strands); (β) triangles with three atoms filled (such configurations are part of zigzag patches); and (γ) triangles with two atoms filled and one empty; such atoms would reside at the edge of a zigzag patch, or at a location where single-atom strands cross over from one side of a double row to the other side. The results of a simulation with values of $\frac{1}{20}:\frac{1}{200}:\frac{1}{2000}$ for the probability of removing the first atom, the adjacent atom, and the opposite atom, respectively, show excellent agreement for the density of the configurations α and β (Fig. 4A),

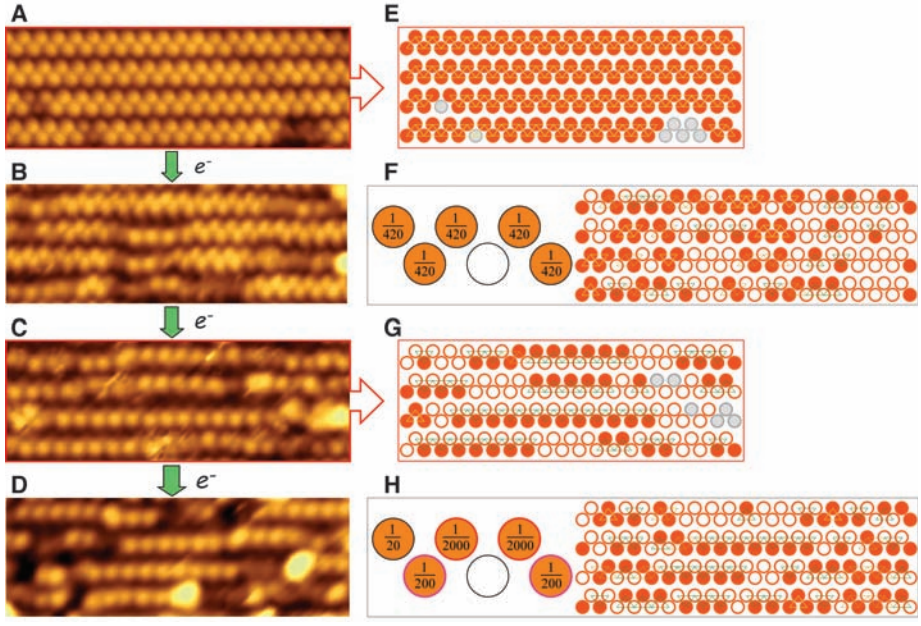

Fig. 3. (**A** to **D**) STM images before (A) and after [(B) to (D)] irradiation with 300-eV electrons. Electron doses and the resulting vacancy concentrations (given as percentages of a monolayer) are (B) 2.3×10^{16} electrons cm^{-2}, 35%; (C) 9.2×10^{16} electrons cm^{-2}, 55%; and (D) 1.8×10^{17} electrons cm^{-2}, 70%. (**E** and **G**) Sketches of the remaining O atoms (orange) and O vacancies (white circles). (**F** and **H**) Monte Carlo simulations of O-vacancy configurations corresponding to (F) a random, first-order desorption process (with an assumed constant yield of one desorbing O atom per 420 incoming electrons), and (H) desorption yields of $\frac{1}{20}:\frac{1}{200}:\frac{1}{2000}$ for the first O atom, an O atom adjacent to an O vacancy, and an O atom opposite an O vacancy, respectively.

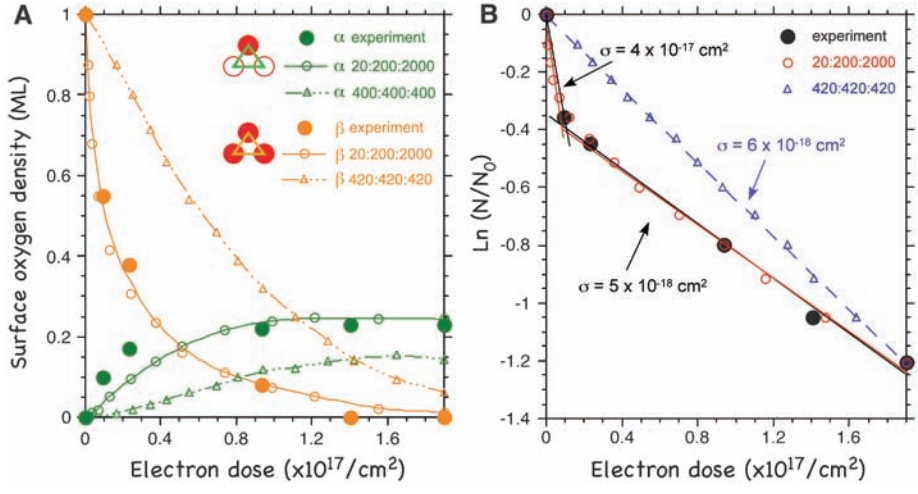

Fig. 4. (**A**) Number of configurations of O atoms with two O vacancies (α) and two oxygen atoms (β) as nearest neighbors, as a function of irradiation with 300-eV electrons. (**B**) Total number of O atoms on the surface versus electron dose. Experimental values are compared with the results of Monte Carlo simulations with the same desorption probabilities as in Fig. 3, F and H. A linear fit in the semilogarithmic plot in (B) allows for an evaluation of the average cross section for electron-stimulated desorption.

the size distribution of the resulting single-atom strands and zigzag patches, and the decrease of the total number of surface O atoms as a function of electron dose (Fig. 4B).

In principle, for a first-order desorption process, a semilogarithmic plot of the number of remaining atoms versus the electron dose would follow a straight line; the slope of the line gives the cross section (triangular points and associated line in Fig. 4B). The experimental data in Fig. 4B deviate from such a behavior. The much more rapid decrease for low electron doses, where atoms are mainly desorbed from pristine areas without O vacancy sites, is well described by our Monte Carlo results (circles in Fig. 4B). Our statistical analysis allows the determination of the site-specific desorption probability on an atom-by-atom basis. In contrast, a signal that is proportional to the total surface O concentration (such as in Fig. 4B), or to the desorbing species, can only be used to determine an average cross section that lumps together the probabilities for all individual desorption events.

The few average cross sections reported for ESD of TiO_2 (*31*, *32*) are of magnitudes similar to that of the average cross section indicated in Fig. 4B. The probability for electron-stimulated desorption from the pristine surface is very high, however. A value of 1 in 20 electrons provides the best fit to all experimental observables; taking into account the parameter values that lie within our confidence value, we determine the initial cross section to be ~9 (±6) × 10^{-17} cm^2 (*33*).

Why is the desorption from the pristine surface so efficient, and why does the proximity to a defect site decrease the probability so effectively? Previous measurements have firmly established that core-hole excitations are connected to O desorption (*19*, *23*); we also find that irradiation with ~25-eV electrons, an energy smaller than the core-level binding energies in TiO_2, does not produce any observable defects on TiO_2(011)-2×1. The cross section for stimulated desorption can be described by $\sigma = I \times P$, where I denotes the cross section for a core-hole ionization, and P is the probability that this excitation results in a desorption event (i.e., an excited state that is both repulsive and long-lived enough to induce nuclear motion). Measured cross sections for Ti 3p ionization of Ti ions in the gas phase vary between 1 × 10^{-17} cm^2 and 9 × 10^{-17} cm^2, depending on the ionization state (*34*, *35*).

Electron backscattering can increase the ionization probability in a solid by up to a factor of 2 relative to the same species in the gas phase; this could be the reason why the measured cross section for O desorption from pristine TiO_2 lies at the upper range of the values for isolated Ti. However, this value implies that the desorption cross section is comparable in magnitude to the cross section for ionization ($\sigma \sim I$) and that the probability for desorption after core-hole excitation, P, must be near unity.

In the K-F model (*19*), the decay of the initial excitation results in the conversion of O^{2-} to O^+. This O^+ ion then finds itself surrounded by positively charged lattice Ti and will be repelled by the reversed Madelung potential. (The O^+ ions can also capture an electron on their way out of the surface and desorb as neutral atoms, as long as the neutralization does not occur too close to the original position, which would quench the emission process.) Classical trajectory calculations of the ion emission process show that ejection from the surface will only occur for highly undercoordinated surface O atoms (*36*); apparently, this is the case on TiO_2(011)-2×1.

What is the probability, then, for a core-hole excitation resulting in a three-hole final state in a surface O atom? Recent electron-ion coincidence spectroscopy measurements (*23*) have helped refine the K-F picture, which relied on a (relatively unlikely) interatomic Auger decay, accompanied by the [also not highly probable (*37*)] emission of two Auger electrons from an O ligand. Calculations of core-hole excitations (*38*), based on a cluster model in the framework of the Anderson impurity model, show that a multihole final state of the ligand is in fact quite probable for early transition metal oxides, even without accounting for a consecutive Auger de-excitation process. The high degree of covalency in ground-state configurations of TiO_2 is expressed as $|c\mathrm{d}^{0+q}L^q\rangle$, where q denotes the number of electrons that have been transferred from the ligand orbital, L, to the (formally empty) d electron shell on the metal atom. In a simple physical picture, the creation of a core hole, c, pulls the 3d band down in energy, and electrons flow from the oxygen ligand to the Ti. For TiO_2 the core-hole final state, $|\underline{c}\mathrm{d}^{0+q}L^q\rangle$, exhibits configurations with q up to 5, with a fractional parentage for $q \geq 3$ of 25% (*38*). Similar values have been reported for other transition metal oxides with a high degree of hybridization (*38*); thus, an excited state that could lead to O desorption is in fact quite probable. It remains to be tested whether the unexpectedly high cross section observed for pristine TiO_2(011)-2×1 is specific to this surface, or if it will occur on other TiO_2 surfaces, or other oxides, as well.

It is well established that an O vacancy on TiO_2 surfaces results in a filled-gap state located ~0.8 eV below the conduction band minimum (*17*). The drastic decrease in the desorption probability for O atoms next to an O vacancy is likely caused by these extra electrons at defect sites "screening" the repulsive excited state. The absence of mobile conduction electrons is the reason why, in general, DIET processes are much more efficient on semiconductors than on metals. The strong site dependence of the screening that results in the distinct one-dimensional rows needs some explanation, however, given that the separations between opposite O neighbors across and parallel to the zigzag rows are not too different (measured values of 4.5 Å and 5.5 Å, respectively). Yet we estimate that the desorption probabilities are reduced by one and two orders of magnitude for an O adjacent and opposite to an O vacancy, respectively. An explanation based on the recent observation of anisotropic conductivity in rutile does not appear to be adequate (*39*).

One possible explanation is quenching of the electronic excitation by defect-induced electronic states. Lattice distortions that occur during the desorption process may enhance this effect. Recent density functional theory calculations give strong evidence that the degree of charge localization of vacancy electrons is sensitively dependent on small distortions within the lattice (*40*). During a desorption event, the lattice starts to distort dynamically (*9*); this could cause electrons in the defect state to flow toward the location of the O atom as it starts to leave the surface. This scenario gives a plausible explanation for the differences in the reduced desorption probability along and across the row of the O vacancy. Nearest O neighbors are much more directly linked, whereas weaker coupling to next-nearest O neighbors makes a sharing of charges, or a charge redistribution during the lattice distortion, less efficient. Thus, the strong anisotropy in the bonding geometry at this particular surface is fundamental for the anisotropic quenching of electronically excited states in the vicinity of O vacancies.

In general, atomic vacancies on dielectric surfaces result in a modification of the local electronic structure. We have shown that this altered electronic configuration causes a strong variation of DIET processes in the vicinity of O vacancies, as excess electrons from the defects slosh toward a neighboring atom that has been put into a repulsive state via a core-hole excitation. Thus, defects have a self-limiting effect in the modification of surfaces, and the resulting self-organization of defect structures can be used to pattern surfaces at the atomic scale. In the case of the anisotropic TiO_2(011) surface, the formation of one-dimensional defect structures is favored; because O vacancies react strongly with molecular and metal adsorbates (*41*, *42*), such structures could be used to template interesting overlayers (e.g., one-dimensional rows of catalytically active Au atoms). Quenching of excitations is expected to be observable not only in the presence of O vacancies; other intrinsic or extrinsic electron donors will have similar effects. This has implications for materials design issues such as increasing the radiation resistance of coatings or optimizing responses of photoactive materials.

References and Notes

1. J. T. Yates Jr. *et al.*, *Science* **255**, 1397 (1992).
2. T. E. Madey, *Science* **234**, 316 (1986).
3. K. Nakayama, J. H. Weaver, *Phys. Rev. Lett.* **82**, 980 (1999).
4. T. E. Madey, D. E. Ramaker, R. Stockbauer, *Annu. Rev. Phys. Chem.* **35**, 215 (1984).
5. B. Such *et al.*, *Phys. Rev. Lett.* **85**, 2621 (2000).

6. J. Herring, A. Aleksandrov, T. M. Orlando, *Phys. Rev. Lett.* **92**, 187602/1 (2004).
7. B. V. Yakshinskiy, T. E. Madey, *Nature* **400**, 642 (1999).
8. M. Lastapis *et al.*, *Science* **308**, 1000 (2005).
9. R. E. Walkup, P. Avouris, *Phys. Rev. Lett.* **56**, 524 (1986).
10. J. R. Hahn, W. Ho, *J. Chem. Phys.* **123**, 214702 (2005).
11. D. Menzel, R. Gomer, *J. Chem. Phys.* **41**, 3311 (1964).
12. P. A. Redhead, *Can. J. Phys.* **42**, 886 (1964).
13. J. A. Misewich, T. F. Heinz, D. M. Newns, *Phys. Rev. Lett.* **68**, 3737 (1992).
14. K. Hashimoto, H. Irie, A. Fujishima, *Jpn. J. Appl. Phys.* **44**, 8269 (2005).
15. T. E. Madey, N. S. Faradzhev, B. V. Yakshinsksiy, N. V. Edwards, *Appl. Surf. Sci.* **253**, 1691 (2006).
16. A. L. Linsebigler, G. Lu, J. T. Yates Jr., *Chem. Rev.* **95**, 735 (1995).
17. U. Diebold, *Surf. Sci. Rep.* **48**, 53 (2003).
18. X.-Q. Gong, A. Selloni, M. Batzill, U. Diebold, *Nat. Mater.* **5**, 665 (2006).
19. M. L. Knotek, P. J. Feibelman, *Phys. Rev. Lett.* **40**, 964 (1978).
20. C. L. Pang *et al.*, *Nanotechnology* **17**, 5397 (2006).
21. Q. Wang, J. Biener, X.-C. Guo, E. Farfan-Arribas, R. J. Madix, *J. Phys. Chem. B* **107**, 11709 (2003).
22. C. Noguera, *Physics and Chemistry of Oxide Surfaces* (Cambridge Univ. Press, Cambridge, 1996).
23. S.-i. Tanaka, K. Mase, S.-i. Nagaoka, *Surf. Sci.* **572**, 43 (2004).
24. T. J. Beck *et al.*, *Phys. Rev. Lett.* **93**, 036104/1 (2004).
25. O. Dulub, C. Di Valentin, A. Selloni, U. Diebold, *Surf. Sci.* **600**, 4407 (2006).
26. X.-Q. Gong, A. Selloni, personal communication.
27. The rutile structure is tetragonal, and the TiO_2(011)/(101) surface is inequivalent to the often-investigated TiO_2(110) surface.
28. S. Wendt *et al.*, *Surf. Sci.* **598**, 226 (2005).
29. C. Di Valentin *et al.*, *J. Am. Chem. Soc.* **127**, 9895 (2005).
30. A. G. Fedorus, E. V. Klimenko, A. G. Naumovets, E. M. Zasimovich, I. N. Zasimovich, *Nucl. Instrum. Methods Phys. Res. B* **101**, 207 (1995).
31. S. A. Joyce, M. Bertino, K. Kim, G. Flynn, *Chemical Structure and Dynamics 1999 Annual Report* (Environmental Molecular Sciences Laboratory, U.S. Department of Energy, 1999) (www.emsl.pnl.gov/docs/annual_reports/csd/annual_report1999/1578b_3f.html).
32. L.-Q. Wang, D. R. Baer, M. H. Engelhard, *Surf. Sci.* **320**, 295 (1994).
33. See supporting material on *Science* Online.
34. P. L. Bartlett, A. T. Stelbovics, *Atomic Data Nuclear Data Tables* **86**, 235 (2004).
35. U. Hartenfeller *et al.*, *J. Phys. B* **31**, 2999 (1998).
36. R. E. Walkup, R. L. Kurtz, *Desorption Induced by Electronic Transitions Diet III* (Springer-Verlag, New York, 1988), pp. 160–166.
37. M. Y. Amus'ya, I. S. Lee, V. A. Kilin, *Phys. Rev. A* **45**, 4576 (1992).
38. R. Zimmermann *et al.*, *J. Phys. Condens. Matter* **11**, 1657 (1999).
39. O. Byl, J. T. Yates Jr., *J. Phys. Chem. B* **110**, 22966 (2006).
40. C. Di Valentin, G. Pacchioni, A. Selloni, *Phys. Rev. Lett.* **97**, 166803/1 (2006).
41. E. Wahlstrom *et al.*, *Phys. Rev. Lett.* **90**, 026101 (2003).
42. T. V. Choudhary, D. W. Goodman, *Appl. Catal. Gen.* **291**, 32 (2005).

43. The Tulane group acknowledges the hospitality of Rutgers University while displaced by Hurricane Katrina, during which time this study was initiated. We thank A. Selloni for useful discussions. Supported by U.S. Department of Energy grants DE-TG02-05ER15702 and DE-FG02-93ER14331, NSF grants CHE-0315209 and CHE-010908, and the Intel Corporation.

Supporting Online Material

www.sciencemag.org/cgi/content/full/317/5841/1052/DC1
Materials and Methods
Figs. S1 and S2
References

8 May 2007; accepted 11 July 2007
10.1126/science.1144787

Dinitrogen Dissociation on an Isolated Surface Tantalum Atom

P. Avenier,[1] M. Taoufik,[1]* A. Lesage,[2] X. Solans-Monfort,[3] A. Baudouin,[1] A. de Mallmann,[1] L. Veyre, J.-M. Basset,[1]* O. Eisenstein,[4] L. Emsley,[2] E. A. Quadrelli[1]*

Both industrial and biochemical ammonia syntheses are thought to rely on the cooperation of multiple metals in breaking the strong triple bond of dinitrogen. Such multimetallic cooperation for dinitrogen cleavage is also the general rule for dinitrogen reductive cleavage with molecular systems and surfaces. We have observed cleavage of dinitrogen at 250°C and atmospheric pressure by dihydrogen on isolated silica surface–supported tantalum(III) and tantalum(V) hydride centers [(≡Si-O)$_2$Ta^{III}-H] and [(≡Si-O)$_2$Ta^{V}H$_3$], leading to the Ta^{V} amido imido product [(≡SiO)$_2$Ta(=NH)(NH$_2$)]: We assigned the product structure based on extensive characterization by infrared and solid-state nuclear magnetic resonance spectroscopy, isotopic labeling studies, and supporting data from x-ray absorption and theoretical simulations. Reaction intermediates revealed by in situ monitoring of the reaction with infrared spectroscopy support a mechanism highly distinct from those previously observed in enzymatic, organometallic, and heterogeneous N_2 activating systems.

Ammonia is the almost exclusive nitrogen source for living organisms, fertilizers and other artificial chemicals, hence making the Haber-Bosch process for ammonia synthesis from dinitrogen among the most relevant heterogeneous catalytic reactions (*1*), with approximately 10^8 tons of ammonia produced yearly (*2, 3*). The catalysts for nitrogen fixation in biological systems are nitrogenase enzymes, which produce yearly about the same amount of ammonia (*2, 3*). These two major catalytic processes, as well as the only well-defined, homogeneous catalyst reported so far (*4*), are structurally and chemically very different. The first is essentially based on a surface of Fe or Ru atoms (*1*), the second on high molecular weight proteins with typically FeMo sulfur clusters (*5*–*7*) and the third on a molecular monometallic molybdenum complex (*4*). Additionally, these systems use different sources of hydrogen (gas phase molecular dihydrogen, NADH, and inorganic acids in solution) and different surrounding "cofactors" [such as inorganic promoters (*1*), coenzymes (*5*), or an organometallic redox system (*4*)] to catalyze the stepwise transformation of dinitrogen to ammonia.

Whether heterogeneous, enzymatic, or homogeneous, all these catalytic processes must entail a succession of elementary steps—involving reactant bond cleavage of the very robust N≡N triple bond and N-H bond formation in the product—possibly mediated by one or more metal atoms. Current understanding of the distinct elementary steps in heterogeneous (*8*, *9*), biochemical (*5*, *6*, *10*), and organometallic (*4*) systems is summarized in Fig. 1. We report herein the observed cleavage of dinitrogen by a silica-supported isolated tantalum atom (*11*, *12*), linked to silica by two (≡Si-O)-Ta bonds and obtained by surface organometallic chemistry (*13*). This N_2 dissociation pathway is unexpectedly different from all the three catalytic systems described above and, more generally, from previously observed surface and solution reactivity patterns.

The dinitrogen activation reported here is based on the use of highly electrophilic electron-deficient Ta hydrides: [(≡Si-O)$_2$Ta^{III}-H] (**1a**) and [(≡Si-O)$_2$Ta^{V}H$_3$] (**1b**) (*11*, *12*). These hydrides have already proven very active in the catalytic transformation of alkanes (e.g., alkane metathesis) by C-H and C-C bond cleavage (*14*, *15*) and more recently in ammonia activation by N-H bond cleavage (*16*). In this latter case, the characterized product was the Ta^{V} amido imido complex [(≡SiO)$_2$Ta(=NH)(NH$_2$)] (**2**), along with its ammonia adduct **2**·**NH$_3$**.

The starting tantalum hydrides **1** are obtained in two steps, which have already been

[1]Université de Lyon, C2P2, Laboratoire de Chimie Organométallique de Surface UMR5265 CNRS-CPE-UCBL1 43, Boulevard du 11 Novembre 1918, BP 2077 F-69616, Villeurbanne Cedex, France. [2]Université de Lyon, Laboratoire de Chimie, UMR-5182 CNRS-ENS, Lyon, Ecole Normale Supérieure de Lyon, F-69364 Lyon Cedex, France. [3]Departament de Química, Universitat Autònoma de Barcelona, 08193 Bellaterra, Spain. [4]Institut Charles Gerhardt, UMR 5253 CNRS, UM 2- ENSCM, UM1, Chimie Théorique, Méthodologies, Modélisations, Université Montpellier 2, F-34095 Montpellier Cedex 05, France.

*To whom correspondence should be addressed. E-mail: quadrelli@cpe.fr (E.A.Q.); taoufik@cpe.fr (M.T.); basset@cpe.fr (J.-M.B.)